Flat field of UVCS detectors for early part of SOHO mission

Mario L. Cosmo*, Peter L. Smith, Nigel Atkins, Raid M. Suleiman, Larry D. Gardner, John L. Kohl

Harvard-Smithsonian Center for Astrophysics, Cambridge, MA 02138

ABSTRACT

The Ultraviolet Coronagraph Spectrometer (UVCS) on the Solar and Heliospheric Observatory (SOHO) comprises two telescopes and two spectrometer channels for spatially resolved ultraviolet spectral diagnostics of the solar corona. The principal lines for which the two channels are optimized are the H I "Lyman-α" line at 121.5 nm and the O VI (O^{5+}) doublet at 103.2 and 103.7 nm. An "in-flight" method, using observations of stars and scattered solar disk light, has been devised to determine the flat field function, i.e., the relative detection efficiency of the detector pixels. We present the details and results of this process. Local pixel-to-pixel efficiency variation is found to be, typically, about ±9% to ±17% (1 σ) for the H I Lyman-α channel and ±9% for the O VI channel.

Keywords: UV spectroscopy, detectors, calibration, flat field

1. INTRODUCTION

The Ultraviolet Coronagraph Spectrometer (UVCS) on the Solar and Heliospheric Observatory (SOHO) was designed for ultraviolet (UV) spectroscopy and visible light polarimetry of the extended solar corona[1]. UV observations are used primarily to determine ion densities as well as random velocity distributions and bulk outflow velocities of neutral H, O^{5+}, and several minor ions in the solar corona. The goal is to investigate the origins and properties of the solar wind as well as mechanisms for heating and accelerating it.

The UV portion of UVCS comprises two telescopes and two stigmatic spectrograph channels designed primarily for measurements of the intensities and profiles of the H I "Lyman-α" (or Ly α) line at 121.5 nm and the O VI (O^{5+}) doublet at 103.2 and 103.7 nm. The channels and their components are designated LYA and OVI, respectively. The spectrograph channels create wavelength-dispersed images of the field of view (FOV) that are detected with crossed delay line (XDL) detectors[2] that have 1024 pixels (25 μm square) in the spectral direction (denoted *c*, for column) and 360 in the spatial direction (denoted *r*, for row). The detector pixels are "virtual"; position information is determined electronically from analog signals. Because of limitations in data transmission, data from only 20,000 pixels, or 20,000 "bins" composed of rectangular arrays of pixels, can be obtained for any exposure. The selected pixels, or bins, are set by a "mask". When binned data are used, spectral and/or spatial range are increased, but there are reductions in spectral and/or spatial resolution.

$Q(\lambda,c,r)$, the detection sensitivity of the pixels of the detectors, is assumed to be comprised of two factors: $q(\lambda)$, the wavelength sensitivity of the KBr detector photocathodes, and $F(c,r)$, which gives the fractional deviation of the response of each detector pixel from the average. Therefore,

$$Q(\lambda,c,r) \equiv q(\lambda)F(c,r),$$

where $F(c,r)$, which has an average value of 1.0 by definition, is called the "flat field". To meet the scientific goals of UVCS, both the overall instrument sensitivity, $\rho(\lambda)$, and any pixel-to-pixel variation in that sensitivity, $F(c,r)$, must be known. Pre- and in-flight measurements of $\rho(\lambda)$ are discussed by Gardner et al.[3]; determination of the detector flat fields for the early years of the mission is the subject of this paper. A more complete discussion of UVCS/SOHO detector flat fields is in preparation.[4]

* Correspondence: E-mail: mcosmo@cfa.harvard.edu; Telephone: 617-495-7412; Fax: 617-496-7670

Part of the SPIE Conference on Ultraviolet and X-Ray Detection, Spectroscopy, and Polarimetry III
Denver, Colorado • July 1999
SPIE Vol. 3764 • 0277-786X/99/$10.00

2. UVCS SOHO FLAT FIELD OBSERVATIONS AND DATA ANALYSIS

Determining *F(c,r)* is called "flat fielding", or calibrating, the detector. Ideally, this can be done by uniformly illuminating the detector with photons at the appropriate wavelengths and noting the pixel-to-pixel response. In orbit flat fielding methods use somewhat normal observationals to provide this illumination in a two-part process. Simply put, the procedure is: (1) to determine the flat field for one or more selected columns of pixels, and then, (2) to determine the response of other columns relative to the selected ones. The order in which these measurements are made is not important.

2.1 Observations of stars; uniform illumination of individual detector columns

By aligning the UVCS/SOHO FOV to the apparent path of a star, we can use the star image to sequentially and uniformly illuminate essentially all the pixels in selected columns of the detectors. Because the stellar intensity is constant, all observed *r* dependence is due to detector effects. However, because stellar spectra contain absorption and/or emission features, the column-to-column illumination is not uniform

There are only two stars that pass through the UVCS/SOHO field of view each year that are bright enough for use in flat fielding the detectors at UV wavelengths: ζ Tau on approximately June 15 and δ Sco on approximately November 22. Because of the limits on data transmission (see §1), observations of these are limited by a mask to 39 columns of spectral pixels at the maximum (1x1 pixel) resolution. Nevertheless, such observations of stars suffice for determining the flat field for selected columns of pixels, i.e., for part (1) of the flat-fielding process. Figure 1 shows a number of star observations taken at a 4 min cadence and the sum of this partial data set.

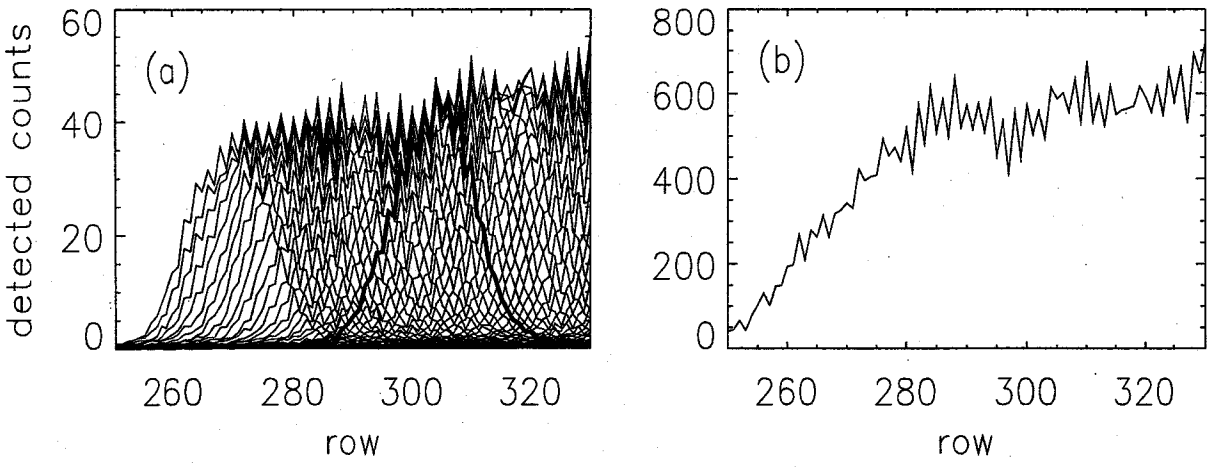

Figure 1: (a) Some of the exposures, averaged over 39 columns, in an observation of δ Sco for a portion of the LYA detector. Data for a representative exposure are plotted in bold so they can clearly be seen. (b) Sum of detected δ Sco observations for a single column of the LYA detector. Note that for this partial data set, the summed data are not useful for rows less than about 285. The row-to-row variation is discussed in the text.

If the detector were "flat" and the data perfect, the summed data for each column would be constant. Deviations from constant values are a result of: (i), counting statistics, and, (ii), the detector non-uniformities that we are trying to determine. One such non-uniformity is immediately obvious from Figure 1: there is a periodic alternation in sensitivity of about ±10 percent from one row of the detector to the next. This anomaly, which is common to both detectors and is thought to be an artifact of the process that converts analog signals to pixel information, is only a minor problem for most UVCS/SOHO science observations because 3x1 (row x column) bins are the smallest employed.

2.2 Observations of scattered solar disk light

2.2.1 Uniform illumination of individual detector rows

The limited flat fields determined with stellar observations are transferred to uncalibrated columns by making a number of observations of some source with a sequence of slightly different settings of the spectrometer grating angles. This "pushbroom" procedure uniformly illuminates adjacent columns of the detector, albeit with a non-uniform intensity in the spatial direction. The source used for this part of the UVCS/SOHO detector flat field determinations is scattered solar disk light that is enhanced by deliberate mispositioning of the internal occulters in the telescopes. The spatial distribution of this illumination, plus photons from the corona that are detected simultaneously, is called the "source function", $S(r,t)$.

Because both the disk and the coronal intensities can vary in time, frequent "reference" observations are required to detect changes in $S(r,t)$. Thus, the procedure for observing scattered disk light is to make two exposures at a reference position, then two similar data exposures at each of ten grating positions that differ by an amount corresponding to 2 columns on the detector, then two exposures at the reference position, etc. Some measurements were made with 1x1 binning; others with 3x1. The reference data for various scattered disk light measurements differed significantly (see Fig. 2).

The data for all columns between the two half-intensity points of these exposures were summed and the resulting column vector was smoothed with a 15 point filter to create the source functions. Examples are shown in Figure 2. The statistical uncertainties for the source functions were about ±2.5% and ±1.4% for the OVI and LYA detectors, respectively. The effects of time dependent changes were removed by dividing each data exposure by time-interpolated values of the source function.

Representative, time-dependence-corrected, scattered disk light data are shown in the top panel of Figure 3. All exposures were then summed, pixel by pixel, to create a preliminary flat field. The average, over rows 50 to 300 (50:300 in the notation of IDL) of a portion of the LYA flat field is shown in the bottom panel of Figure 3.

2.2.2 Discussion

Theanomalies in the summed data at, approximately, columns 654 and 674 are caused by mask edge effects that are visible in the unsummed data (see lower edge of top panel of Fig. 3). The wings of some of the Ly α profiles fell outside the limits of the masks and the resulting data were not transmitted to the ground. There are also mask edge effects at columns 634 and 694, but these are somewhat obscured in Figure 3 by being in the non-flat portion of the summed data. Mask edge effects were removed by summing the data over the central 250 rows of the detector, fitting that sum with a 5-term polynomial to remove the high-frequency, mask-edge-caused, effects, and then multiplying the data in each row by the ratio fit/sum.

When observing scattered disk light with the LYA detector, H I Ly α photons at 121.5 nm dominate. However, with the OVI detector, three lines (H I Ly β at 102.6 nm and O VI at 103.2 and 103.7 nm) are seen. To simplify the data analysis, the OVI scattered disk light exposures were chopped so that only the central portion (between the FWHM points) of the 103.2 nm line profile was used.

2.3 Combining stellar and scattered disk light observations

The summed, time-dependence-corrected, scattered disk light data give a rough approximation, $F'(c,r)$, to the flat fields. These data are, in fact, the flat fields relative to the average flat fields for the portions of the detector used for the reference exposures. To get the true flat fields, we compare $F'(c,r)$ to $F(c,r)$ for the columns used to observe stars. The correction factor, F/F' averaged over these columns, is used to produce a final flat field. For convenience, it is normalized to give an average value of 1.0 for portions of the detector without major flaws or damage. All calculations were done with 1x1 bins, but, because most scattered disk light measurements were obtained with 3x1 (row x column) bins, most flat field results are relevant only on that scale. Therefore, the flat field files were rebinned to 3x1 for analysis of scientific data.

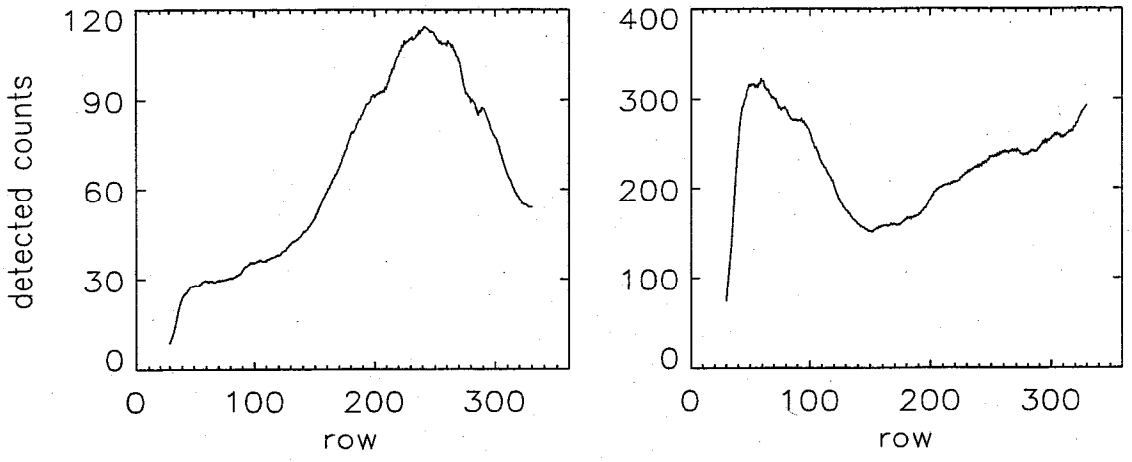

Figure 2: LYA source function for October 1996 (a) and April 1997 (b) scattered disk light observations. OVI source functions were similar in shape, but not in intensity. Values plotted are averages over the central 25 columns of the spectral profile (12 columns FWHM) smoothed with a 15-point filter in the spatial direction.

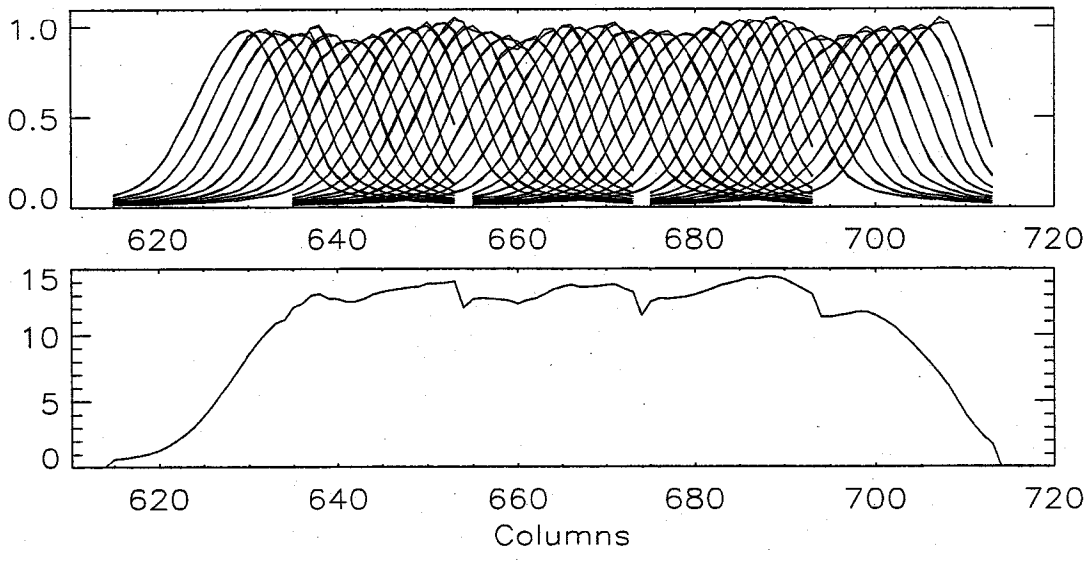

Figure 3. (top panel) 80 scattered disk light exposures, two at each grating position, for the LYA detector. Each exposure has been divided by a time-interpolated value of the appropriate reference exposure and averaged over rows 50:300. (Bottom panel) Sum of scattered disk light exposures in top panel.

3. RESULTS AND DISCUSSION

3.1 LYA detector prior to September 1997

The scattered disk light measurements for the LYA detector were obtained in two segments: (i) columns 430:810 using 1x1 bins and (ii), columns 230:485 and 790:890 using 3x1 bins (all ranges being approximate). The resulting flat field in shown in Figure 4. The pixel-to-pixel deviations from the local mean values (typically over 100x100 pixels) of the flat field ranged from ±9% (one standard deviation) for the portion of the detector centered at row 150 and column 700 to ±17% for the portion centered at row 100 and column 500. A small amount of this scatter is a result of measurement uncertainty, which is discussed in §3.3.

3.2 OVI detector

The OVI flat field is shown in Figure 5. This detector has a positively charged wire grid in front of its photocathode that prevents stray ions from reaching the detector. (The LYA detector is sealed with a MgF_2 window, so ions are not a problem.) The wires in the spatial direction are clearly visible in Figure 5; those in the spectral direction are out of focus but contribute nevertheless to the flat field in a manner that is discussed in §3.3. The bin-to-bin deviation from the mean value is about ±9% for the OVI detector. A significant fraction of that scatter is actually systematic, at least in the column direction: it is caused by the out-of-focus images of the wires that impose a periodic modulation – too subtle to see in Figure 5 – on the flat field.

3.3 Uncertainties

The process of flat fielding the detector requires three sets of data: star observations, scattered disk light observations, and the reference observations used to determine the source function. All contribute statistical uncertainty to the results.

The statistical uncertainties in the preliminary flat field produced from the scattered disk light observations and the source functions are between 2 and 3% for the LYA detector and between 4 and 5% for the OVI one. The statistical uncertainties in the star data were 2 to 4%, depending upon the detector. To minimize the effects of defects in the part of the detector used for the star observations, 20 or more columns were used to normalize the preliminary flat field obtained from the scattered disk light data. The impact of the uncertainties in the star data on the final results were less than 1%. Thus, the measurement uncertainties have only a small effect on the flat fields, and the observed pixel-to-pixel scatter in the flat fields give a good, though slightly too large, estimate of the actual scatter in detector performance.

3.4. Changes in the detectors

Microchannel-plate-based detectors have a limited lifetime. After a certain number of events have produced amplified pulses in a channel, the number of electrons in the charge clouds produced in that channel starts to decrease. Eventually, some of the pulses fall below the discriminator setting in the position determining electronics; these pulses are not counted, so there is an effective loss of detector efficiency. For the OVI detector, changes in performance to date appear to be minor. For the LYA detector, there were no major changes prior to September 1997, but significant decreases in efficiency have been noted for heavily used portions following a decrease in the detector bias voltage at that time. These effects are discussed by Smith et al.[4]

Because such changes occur, it is important to note that the flat field determinations discussed above are essentially "snapshots" indicating detector performance at a certain time. In fact, since the data used to calibrate the detectors were obtained over a number of months, the flat fields are really "mosaics", with data for different parts of the detector being relevant for a number of specific different epochs. Because the UVCS/SOHO detector flat fields are dynamic, i.e., they change with use of the detector, users should consult the UVCS webpage http://cfa-www.harvard.edu/uvcs/ for up-to-date information about flat fields for different periods.

ACKNOWLEDGEMENTS

The UVCS/SOHO Program is supported by the National Aeronautics and Space Administration under contract NAS5-7822 to the Smithsonian Astrophysical Observatory, by the Agenzia Spaziale Italiana, and by Swiss funding agencies.

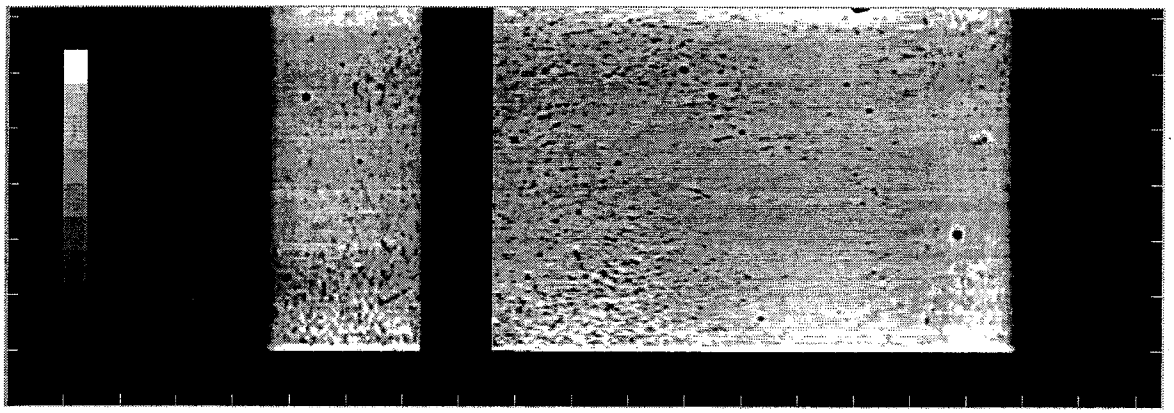

Figure 4: LYA detector flat field prior to September 1997. Because of changes in operating parameters, this flat field on only relevant for this period (see §3.4). The fiducial marks are at 50 pixel increments. The inset at columns 50:70 shows the relative sensitivity scale: 1.2, 1.1, 1.0, 0.9, etc., as one moves downwards. The gap at columns 370:430 shows the position of a deliberately blocked portion of the detector.

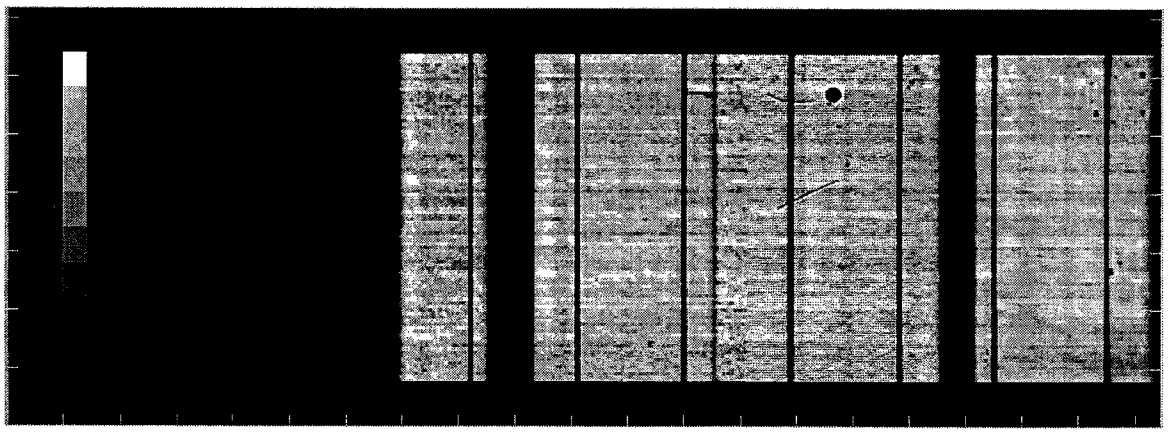

Figure 5: UVCS OVI detector flat field. The portion of the detector above column 860 is used for "redundant" detection of Ly-α photons, which are focussed there by an extra mirror in the OVI channel. The fiducial marks are at 50 pixel increments. The inset at columns 50:70 shows the relative sensitivity scale: 1.2, 1.1, 1.0, 0.9, etc., as one moves downwards. Most narrow vertical stripes are the images of the wire grid (see text), but the one at columns 625:630 results from edge effects where two large data sets, not quite complete, were merged. The wide gap near column 450 is also a result of missing data.

REFERENCES

1. Kohl, J. L., Esser, R., Gardner, L. D., Habbal, S., Daigneau, P. S., Dennis, E. F., Nystrom, G. U., Panasyuk, A., Raymond, J. C., Smith, P. L., Strachan, L., van Ballgooijen, A. A., Noci, G., Fineschi, S., Romoli, M., Ciaravella, A., Modigliani, A., Huber, M. C. E., Antonucci, E., Benna, C., Giordano, S., Tondello, G., Nicolosi, P., Naletto, G., Pernechele, C., Spadaro, D., Poletto, G., Livi, S., von der Luhe, O., Geiss, J., Timothy, J. G., Gloeckler, G., Allegra, A., Basile, G., Brusa, R., Wood, B., Siegmund, O. H. W., Fowler, W., Fisher, R., Jhabvala, M., "The Ultraviolet Coronagraph Spectrometer for the Solar and Heliospheric Observatory," *Solar Physics*, **162**, pp. 313-356, 1995.

2. Siegmund, O. H., Stock, J. M., Marsh, D. R., Gummin, M. A., Raffanti, R., Hull, J., Gaines, G. A., Welsh, B. Y., Donakowski, B., Jelinsky, P. N., Sasseen, T., Tom, J. L., Higgins, B., Magoncelli, T., Hamilton, J. W., Battel, S. J., Poland, A. I., Jhabvala, M. D., Sizemore, K., Shannon, J. "Delay line detectors for the UVCS and SUMER instruments on the SOHO satellite," *Proc. SPIE* **2280**, p. 89-100 , 1994.

3. Gardner, L. D., Kohl, J. L., Daigneau, P. S., Dennis, E. F., Fineschi, S., Michels, J., Nystrom, G. U., Panasyuk, A., Raymond, J. C., Reisenfeld, D. J., Smith, P. L., Strachan, L., Suleiman. R., Noci, G. C., Romoli, M. Ciaravella, A., Modigliani, A., Huber, M. C. E, Antonucci, E., Benna, C., Giordano, S., Tondello, G., Nicolosi, P., Naletto, G., Pernechele, C., Spadaro, D., Siegmund, O. H., Allegra, A., Carosso, P. A., Jhabvala, M. D., "Stray light, radiometric, and spectral characterization of UVCS/SOHO: laboratory calibration and flight performance," *Proc. SPIE* **2831**, pp. 2-24, 1996.

4. Smith, P. L., Cosmo, M. L., Atkins, N., Suleiman, R. M., Gardner, L. D., and Kohl, J. L., "In flight determination of flat fields for UVCS/SOHO detectors", in preparation.